

Laser assisted Breit-Wheeler and Schwinger processes

T. Nousch,^{1,2} A. Otto,^{1,2} D. Seipt,^{3,4} B. Kämpfer,^{1,2} A. I. Titov,⁵
D. Blaschke,^{5,6,7} A. D. Panferov,⁸ and S. A. Smolyansky⁸

¹*Institute of Radiation Physics, Helmholtz-Zentrum Dresden-Rossendorf,
Bautzner Landstraße 400, 01328 Dresden, Germany*

²*Institut für Theoretische Physik, Technische Universität Dresden,
Zellescher Weg 17, 01062 Dresden, Germany*

³*Helmholtz-Institut Jena, Fröbelstieg 3, 07743 Jena, Germany*

⁴*Theoretisch-Physikalisches Institut, Friedrich-Schiller-Universität Jena,
Max-Wien-Platz 1, 07743 Jena, Germany*

⁵*Bogoliubov Laboratory for Theoretical Physics, JINR Dubna,
Joliot-Curie str. 6, 141980 Dubna, Russia*

⁶*Institute for Theoretical Physics, University of Wrocław,
pl. M. Borna 9, 50-204 Wrocław, Poland*

⁷*National Research Nuclear University (MEPhI),
Kashirskoe Shosse 31, 115409 Moscow, Russia*

⁸*Department of Physics, Saratov State University, 410071 Saratov, Russia*

(Dated: March 7, 2022)

Abstract

The assistance of an intense optical laser pulse on electron-positron pair production by the Breit-Wheeler and Schwinger processes in XFEL fields is analyzed. The impact of a laser beam on high-energy photon collisions with XFEL photons consists in a phase space redistribution of the pairs emerging in the Breit-Wheeler sub-process. We provide numerical examples of the differential cross section for parameters related to the European XFEL. Analogously, the Schwinger type pair production in pulsed fields with oscillating components referring to a superposition of optical laser and XFEL frequencies is evaluated. The residual phase space distribution of created pairs is sensitive to the pulse shape and may differ significantly from transiently achieved mode occupations.

I. INTRODUCTION

The growing availability of x-ray free electron lasers (XFELs) worldwide stimulates rethinking of elementary quantum processes in which pairs of particles and anti-particles, e.g. electrons (e^-) and positrons (e^+), are created. An avenue to pair creation is the conversion of light (γ) into matter in the collision of (high energy) photon beams. The Breit-Wheeler process, for instance, is the reaction $\gamma' + \gamma \rightarrow e^+ + e^-$, being a crossing channel of the Compton process or the time-reversed annihilation. The famous experiment E-144 [1] can be interpreted as a two-step process with (i) Compton backscattering of an optical laser off the SLAC electron beam and (ii) subsequent reaction of the high-energy Compton-backscattered photons with the same laser beam, producing the pair. While the complete sequence of reactions is named trident process, step (ii) refers to Breit-Wheeler pair production. The notion non-linear Breit-Wheeler process means the instantaneous reaction with a multiple of laser beam photons. A particular variant thereof is the laser assisted Breit-Wheeler process $\gamma' + \gamma_{XFEL} + \gamma_L \rightarrow e^+ + e^-$, i.e. the pair creation in the collision of a probe photon $\gamma_{X'}$ with co-propagating XFEL (γ_{XFEL}) and laser (γ_L) beams.

In contrast to pair creation in counter propagating null fields, also other electromagnetic fields qualify for pair production. An outstanding example is the Schwinger effect originally meaning the instability of a spatially homogeneous, purely electric field with respect to the decay into a state with pairs and a screened electric field [2] (cf. [3] for a recent review). The pair creation rate $\propto \exp\{-\pi E_c/|\mathbf{E}|\}$ for electric fields \mathbf{E} attainable presently in mesoscopic laboratory installations is exceedingly small since the Sauter-Schwinger (critical) field strength $E_c = m^2/|e| = 1.3 \times 10^{16}$ V/cm for electrons/positrons with masses m and charges $\pm e$ is so large (we employ here natural units with $c = \hbar = 1$). Since the Coulomb fields accompanying heavy and super-heavy atomic nuclei or ions in a near-by passage can achieve $\mathcal{O}(E_c)$, the vacuum break down for such configurations with inhomogeneous static or slowly varying fields have been studied extensively [4–8]. Experiments, however, were not yet conclusive.

An analogous situation is met where a spatially homogeneous electric field has a time dependence. The particular case of a periodic field is dealt with in [9] with the motivation that tightly focused laser beams can provide high field strengths. The superposition of a few laser beams, as considered, e.g. in [10], can enlarge the pair yield noticeably. A

particular variant is the superposition of strong optical laser beams and weaker but high-frequency (XFEL) beams. If the frequency of the first field is negligibly small while that of the second field is sufficiently large, the tunneling path through the positron-electron gap is shortened by the assistance of the multi-photon effect and, as a consequence, the pair production is enhanced. This is the dynamically assisted Schwinger process [11]. As assisted dynamical Schwinger effect one can denote the pair creation (vacuum decay) where the time dependence of both fields matters. Many investigations in this context are constrained to spatially homogeneous field models, that is to the homogeneity region of anti-nodes of pairwise counter propagating and suitably polarized beams. Accounting for spatial gradients is much more challenging [12, 13].

Other field combinations, e.g. the nuclear Coulomb field and XFEL/laser beams, are also conceivable [14, 15], but will not be addressed here (cf. [16] for a survey).

A few of the above quoted field configurations share as a common feature the pair creation in bi-frequent fields, as provided by the superposition of optical laser and XFEL beams. Accordingly, we are going to consider the laser assisted Breit-Wheeler and dynamical Schwinger processes in such bi-frequent fields. Our paper is organized as follows. Section 2 deals with the laser assisted Breit-Wheeler process, where spectral caustics have been identified already in [17, 18]. Specifically, we deliver here as new result the phase space distribution of positrons, in particular the double-differential cross section as a function of longitudinal and transverse momenta. In section 3 we consider the assisted dynamical Schwinger effect for the superposition of two spatially homogeneous fields of different strengths and frequencies with a common pulse envelope, as investigated in [18–21]. Here we present for the first time examples of the time evolution to show the striking difference of the transient mode occupancy in an adiabatic basis and the residual phase space yield. The summary and discussion can be found in section 4.

II. LASER ASSISTED BREIT-WHEELER PROCESS

The laser assisted, non-linear Breit-Wheeler process is dealt with within the strong-field QED (Furry picture) as decay of a probe photon traveling through a null field A , symbolically $\gamma' \rightarrow e_A^+ + e_A^-$ where e_A^\pm denote Volkov solutions of the Dirac equation in a plane wave with

vector potential

$$A^\mu(\phi) = \hat{a}_X f_X(\phi) \varepsilon_X^\mu \cos \phi + \hat{a}_L f_L(\eta\phi) \varepsilon_L^\mu \cos \eta\phi. \quad (1)$$

The field (1) is a classical background field, while the probe photon belongs to a quantized radiation field. The XFEL (frequency ω_X , four-momentum k_X^μ , intensity parameter $a_0^{(X)} = \hat{a}_X |e|/m$, polarization four-vector ε_X^μ) and laser (frequency $\omega_L = \eta\omega_X$, intensity parameter $a_0^{(L)} = \hat{a}_L |e|/m$, polarization four-vector ε_L^μ) beams are co-propagating and their linear polarizations are perpendicular to each other. Both beams are pulsed as described by the envelope functions $f_X = \exp\{-\phi^2/(2\tau_X^2)\}$ and $f_L = \cos^2(\pi\phi/(2\tau_L))$ for $-\tau_L \leq \phi \leq +\tau_L$ and zero elsewhere. The invariant phase is $\phi = k_X \cdot x$ with a dot indicating the scalar product of the four-wave vector k_X and the space-time coordinate x .

The theoretical basis for formulating and evaluating the cross section (as well as the corresponding kinematics) is described in Ref. [17]. It reads:

$$\frac{d\sigma}{dp_\perp dp_\parallel d\varphi} = \frac{e^2 p_\perp}{(4\pi)^3 p_0 \rho_X j_{in} k_X \cdot (k_{X'} - p)} \sum_{spins} |\mathcal{M}|^2 \quad (2)$$

with matrix element $\mathcal{M} = \int d^4x \bar{\Psi}_A \not{\varepsilon}_{X'} \exp\{ik_{X'} \cdot x\} \Psi_A$, Ψ_A is the Volkov solution in the external classical field A from (1) and $\bar{\Psi}_A$ its adjoint, and $\varepsilon_{X'}$ denotes the four-polarization of the probe photon X' (four-momentum $k_{X'}$) which will be averaged. We normalize with the particle density $\rho_X = m^2 a_X^2 / (2e^2) \int_{-\infty}^{\infty} d\phi f_X^2(\phi)$ and by the incoming photon flux $j_{in} = k_X \cdot k_{X'} / (k_X^0 k_{X'}^0)$ such that without the laser assistance, Eq. (2) recovers the standard Breit-Wheeler cross section. Examples for the transverse momentum (p_\perp) distribution of positrons are presented in [17, 18] for selected values of the longitudinal momentum p_\parallel at azimuthal angle $\varphi = \pi$ measured w.r.t. the laser polarization plane.¹

To complete the information on the phase space distribution we display the double-differential cross section $d\sigma/dp_\perp dp_\parallel d\varphi$ at $\varphi = \pi/2$ and π as a contour plot over the $p_\perp - p_\parallel$ plane, see Figs. 1 and 2. The ridges as loci of accumulated intensity are interpreted in line with [22] as spectral caustics related to stationary phase points. The impact of the laser consists of a redistribution of Breit-Wheeler-produced pairs in the phase space. Without the laser (this means $\hat{a}_L = 0$) the spectrum becomes much simpler and squeezed to a narrow region (see upper row in Fig. 1 for $a_0^{(L)} = 0.01$), and only the finite pulse length τ_X has imprints on the spectral distribution [23–25]. With increasing laser intensity,

¹ p_\parallel is parallel to the laser plane and p_\perp perpendicular to it.

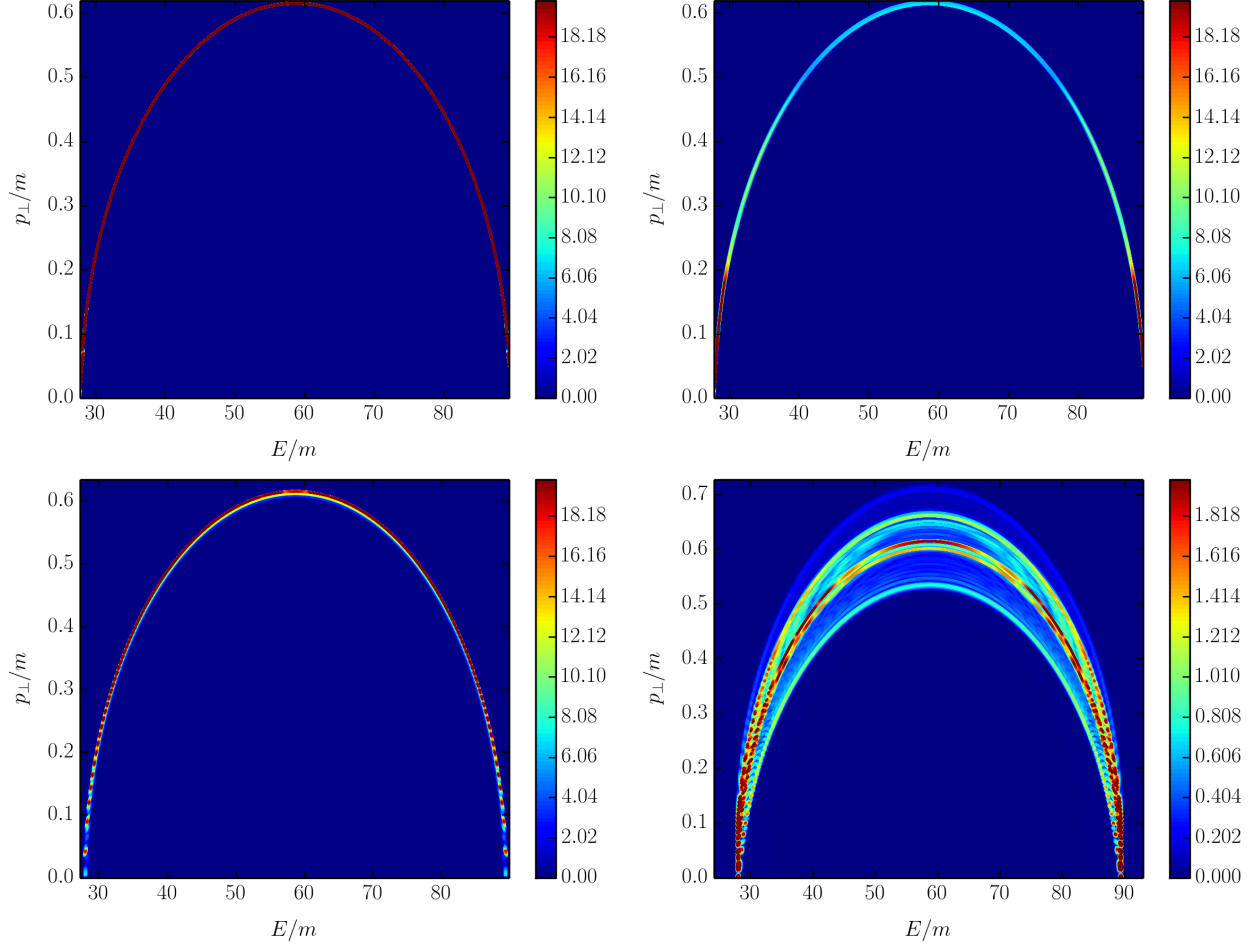


Figure 1. Color-contour plots of the phase space distribution of positrons in a plane aligned to the laser polarization by $\varphi = 0.5\pi$ (left panels) and in the laser polarization plane, i.e. at $\varphi = \pi$ (right panels), as well as $a_0^{(L)} = 0.01$ (upper panels) and $a_0^{(L)} = 0.1$ (lower panels). Transverse momentum p_\perp and energy $E = (m^2 + p_\perp^2 + p_\parallel^2)^{\frac{1}{2}}$ are scaled by the electron mass m . Parameters: $\omega_{X'} = 60$ MeV, $\omega_X = 6$ keV, $\omega_L = 10$ eV, $\tau_L = 4\pi$, $\tau_X = 7/\eta$. Note that $a_0^{(X)}$ does not enter the cross section since we consider here the leading order contribution in an expansion in powers of $a_0^{(X)} \ll 1$, which applies for present XFEL facilities [26].

parametrized by $a_0^{(L)}$ or \hat{a}_L , the spectra become stretched, both in p_\perp and p_\parallel (respective energy E) directions, see bottom row in Fig. 1 and both rows in Fig. 2. The effect of the laser assistance is strongest in the polarization plane of the laser for moderate intensities. Due to the Lorentz force, at larger intensities, also the off-plane becomes populated, see left columns in Fig. 2.

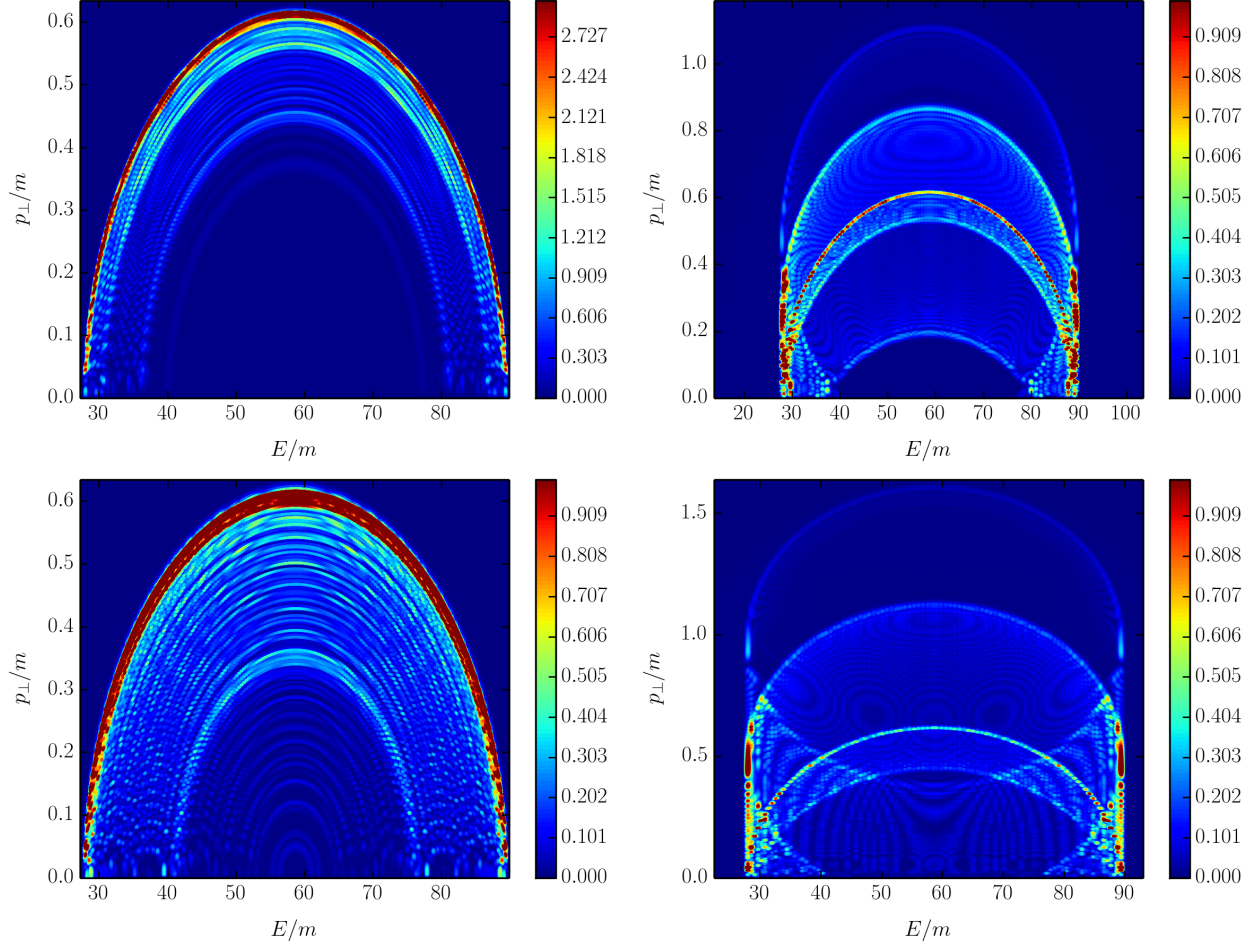


Figure 2. Same as Fig. 1 but for $a_0^{(L)} = 0.5$ (upper panels) and $a_0^{(L)} = 1$ (lower panels).

III. ASSISTED DYNAMICAL SCHWINGER PROCESS

Let us now discuss the time-evolution of the assisted Schwinger pair-production process in bi-frequent laser pulses. The quantum kinetic equation [27]

$$\frac{d}{dt}f(\mathbf{p}, t) = \frac{1}{2}\lambda(\mathbf{p}, t) \int_{-\infty}^t dt' \lambda(\mathbf{p}, t') (1 - 2f(\mathbf{p}, t')) \cos \theta(\mathbf{p}, t, t') \quad (3)$$

determines the time (t) evolution of the dimensionless phase space distribution function per spin projection degree of freedom $f(\mathbf{p}, t) = d^6 N(\mathbf{p}, t) / d^3 p d^3 x$ from a vacuum state $f(\mathbf{p}, t \rightarrow -\infty) = 0$. Here, the quantities $\lambda(\mathbf{p}, t) = eE(t) \varepsilon_{\perp}(p_{\perp}) \varepsilon^{-2}(\mathbf{p}, t)$ stand for the vacuum transition amplitude, and $\theta(\mathbf{p}, t, t') = 2 \int_{t'}^t d\tau \varepsilon(\mathbf{p}, \tau)$ for the dynamical phase; the quasi-energy ε , the transverse energy ε_{\perp} and the longitudinal quasi-momentum P are defined by $\varepsilon(\mathbf{p}, t) = \sqrt{\varepsilon^2(p_{\perp}) + P^2(p_{\parallel}, t)}$, and $\varepsilon_{\perp}(p_{\perp}) = \sqrt{m^2 + p_{\perp}^2}$, $P(p_{\parallel}, t) = p_{\parallel} - eA(t)$, where

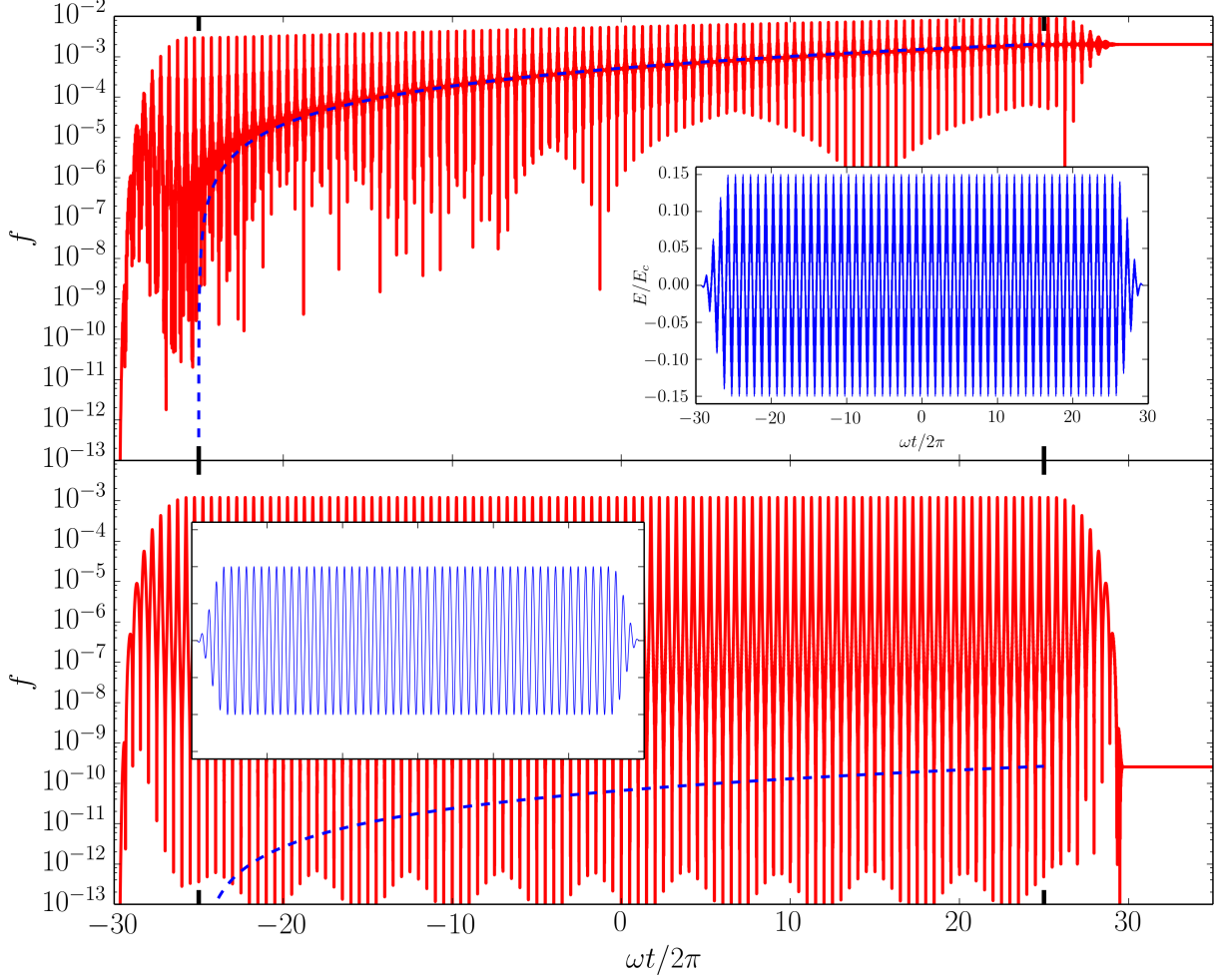


Figure 3. Time evolution of $f(p_{\perp}, p_{\parallel}, t)$ (solid curves, note the variation over many orders of magnitude) from the full quantum kinetic equation (3) for the same envelope function K in (4) as in [19, 20]. The dashed curves in the flat-top interval $-t_{\text{f.t.}}/2 < t < t_{\text{f.t.}}/2$ (marked by bold ticks) are for the relevant component f_{rel} of f (defined in (5-7)) which becomes asymptotically the residual yield. Note that $df/dt = 0$ for $t > t_{\text{f.t.}}/2 + t_{\text{ramp}}$ according to (3) since the external field vanishes. The insets display the time structure of the electric fields. For $\omega t_{\text{ramp}} = 5 \cdot 2\pi$, $\omega t_{\text{f.t.}} = 50 \cdot 2\pi$, $E_1 = 0.1E_c$, $\omega = 0.02m$, $p_{\parallel} = 0$. Further parameters are $E_2 = 0.05E_c$, $N = 25$, $p_{\perp} = 0.155325m$ (upper panel) and $E_2 = 0$, $p_{\perp} = 0.161900m$ (lower panel, the same inset labels and axes ranges as in upper panel inset).

$p_{\perp} = |\mathbf{p}_{\perp}|$ is the modulus of the momentum component perpendicular to the electric field, and p_{\parallel} denotes the \mathbf{E} -parallel momentum component. The electric field $E = -\dot{A}$ in Coulomb

gauge follows from the potential model

$$A = K(\omega t) \left(\frac{E_1}{\omega} \cos(\omega t) + \frac{E_2}{N\omega} \cos(N\omega t) \right). \quad (4)$$

Equation (4) describes again a classical, spatially homogeneous, bi-frequent field with frequency ratio N (integer) and field strengths E_1 – the strong field “1” – and E_2 – the weak field “2”. The quantity K is the common envelope function with the properties (i) flat in the flat-top time interval $-t_{f.t.}/2 < t < +t_{f.t.}/2$ and (ii) zero for $t < -t_{f.t.}/2 - t_{ramp}$ and $t > t_{f.t.}/2 + t_{ramp}$ and (iii) smooth everywhere, i.e. K belongs to the C^∞ class; t_{ramp} is the ramping duration characterizing the switching on/off time intervals (see [19, 20] for details; other envelopes are dealt with in [21]; carrier envelope phase effects and further effects of different envelope models deserve further dedicated investigations). We emphasize the unavoidable ambiguity of a particle definition at intermediate times [28], i.e. only $f(p_\perp, p_\parallel, t \rightarrow +\infty)$ can be considered as a single particle distribution which may represent the source term of a subsequent time evolution. Screening and back reaction need not to be included for small values of f .

Examples of the residual phase space distribution $f(p_\perp, p_\parallel, t \rightarrow +\infty)$ can be found in [19, 20]. In essence, for large enough values of N , the field E_2 enhances the yield achievable by the field E_1 alone. The enhancement can be gigantic, but field strengths E_1 in the order of such ones envisages in ELI-IV [29, 30] and beyond HiPER [31] and sufficiently large N are required to overcome the exponential suppression of pair production in sub-critical fields. The enhancement by a second, high-frequency field is in agreement with a general statement in [32]: The pair production probability is increased by temporal inhomogeneities.

It is instructive to inspect the approach to the residual distribution $f(p_\perp, p_\parallel, t \rightarrow +\infty)$ by means of Eq. (3). Figure 3 exhibits examples of the time evolution of f (solid curves) in two phase space points $p_\perp = p_\ell$, $p_\parallel = 0$ where a resonance condition (cf. [20] for the definition of a series of p_ℓ values) is fulfilled. The upper panel is for a bi-frequent field, while the lower panel is for a single field. Note the large difference of the residual phase space occupancy upon the assistance of a weak but fast field “2”. There are rapid oscillations with huge maximum values at transient times which, however, drop significantly upon switching off the external field. In [20] an approximation has been presented which allows to follow a particularly relevant component of f , f_{rel} (dashed curves), which becomes the residual yield

at $t \rightarrow \infty$:

$$f(p_\ell, 0, t) \approx f_{\text{osc}}(p_\ell, 0, t) + f_{\text{rel}}(p_\ell, 0, t), \quad (5)$$

$$f_{\text{rel}}(p_\ell, 0, t) = \frac{1}{2}|F_\ell|^2 t^2, \quad (6)$$

$$F_\ell = \frac{\omega}{2\pi} \int_0^{2\pi/\omega} dt \lambda(p_\ell, 0, t) e^{i\theta(p_\ell, 0, t, 0)}, \quad (7)$$

where f_{osc} refers to the irrelevant oscillating part and F_ℓ is a Fourier coefficient in the low-density approximation (cf. [19]). In fact, the dashed curves give a remarkably accurate estimate of the final value, irrespectively of details of the ramping and de-ramping as long as the slowly varying envelope approximation is applicable and $t_{f.t.} \gg t_{\text{ramp}}$. Large differences of the residual yields in neighboring phase space points point to resonance type structures.

IV. SUMMARY AND DISCUSSION

In summary we have extended our previous studies [19–21] and deliver here further important details of (i) the phase space distribution in the laser assisted Breit-Wheeler process and (ii) the time evolution of the mode occupancy in the assisted dynamical Schwinger effect. Both topics are motivated by the availability of x-rays by XFELs and upcoming ultra-high intensity laser beams. We consider the perspectives offered by the combination of both beam types resulting in bi-frequent fields.

The laser assisted Breit-Wheeler process is studied for the head-on collision of a probe photon beam with two co-propagating beams, provided by an optical laser (L) and an XFEL (X). Despite of the coherence of the XFEL beam, its intensity parameter $a_0^{(X)}$ is small, thus calling for a restriction of leading order effects in powers of $a_0^{(X)}$. The treatment of misalignment effects of the L and XFEL beams as well as higher order effects in $a_0^{(X)}$ is left for future work, as the investigations of realistic focal spot geometries in focused beams and general polarization effects as well as carrier envelope phase effects. The beams considered here are represented by null fields with large frequency ratios: $\omega_{X'} = \mathcal{O}(60 \text{ MeV})$, $\omega_X = \mathcal{O}(6 \text{ keV})$ and $\omega_L = \mathcal{O}(10 \text{ eV})$ in the laboratory. The impact of the laser L consists essentially in a reshuffling of the phase space distribution for the considered parameters.

Our analysis of the dynamical Schwinger process is based on a very special background field model assuming that spatial inhomogeneities can be neglected. Assuming further that

pair production happens in a spatial region of the dimension of the electron Compton wave length, the often posed idea refers to such a small region in the anti-nodes of a standing wave created by counter propagating and suitably polarized laser beams, where essentially an oscillating electric field occurs. Having in mind the principal interest in the Schwinger effect as genuinely non-perturbative quantum decay of the vacuum, we stay with such a model and extend it to a bi-frequent field. To overcome the exponential suppression of pair creation one has to combine a near-critical, low-frequency (laser) field and a sub-critical, high-frequency field, the latter one corresponding more to γ radiation than x-rays. We expect that deviations from the considered idealization will diminish the pair yield, despite of potentially huge enhancement effects due to the assistance of a second field. An interesting question concerns the speculation whether the fairly large transient mode occupation can be probed, e.g. via secondary signals or active probes.

ACKNOWLEDGMENTS

R. Sauerbrey, T. E. Cowan and H. Takabe are gratefully acknowledged for the collaboration within the HIBEF project [33]. We thank S. Fritzsche and A. Surzhykov for the common work on the caustic interpretation of elementary QED processes in bi-frequent fields. D.B. and S.A.S have been supported by Narodowe Centrum Nauki under grant number UMO-2014/15/B/ST2/03752.

We dedicate this article to Walter Greiner on the occasion of his 80th birthday. Walter Greiner promoted essentially the in-depth exploration of the nature of the quantum vacuum.

-
- [1] D. L. Burke *et al.*, Phys. Rev. Lett. **79**, 1626 (1997).
 - [2] J. Schwinger, Phys. Rev. **82**, 664 (1951).
 - [3] F. Gelis and N. Tanji, arXiv:1510.05451 (2015).
 - [4] J. Rafelski, B. Müller, and W. Greiner, Z. Phys. A **285**, 49 (1978).
 - [5] J. Rafelski, L. P. Fulcher, and W. Greiner, Phys. Rev. Lett. **27**, 958 (1971).
 - [6] B. Müller, H. Peitz, J. Rafelski, and W. Greiner, Phys. Rev. Lett. **28**, 1235 (1972).
 - [7] B. Müller, J. Rafelski, and W. Greiner, Phys. Lett. B **47**, 5 (1973).

- [8] F. Fillion-Gourdeau, E. Lorin, and A. D. Bandrauk, *J. Phys. B* **46**, 175002 (2013).
- [9] E. Brezin and C. Itzykson, *Phys. Rev. D* **2**, 1191 (1970).
- [10] N. B. Narozhny, S. S. Bulanov, V. D. Mur, and V. S. Popov, *Phys. Lett. A* **330**, 1 (2004).
- [11] R. Schützhold, H. Gies, and G. Dunne, *Phys. Rev. Lett.* **101**, 130404 (2008).
- [12] G. V. Dunne and C. Schubert, *Phys. Rev. D* **72**, 105004 (2005).
- [13] M. Ruf, G. R. Mocken, C. Müller, K. Z. Hatsagortsyan, and C. H. Keitel, *Phys. Rev. Lett.* **102**, 080402 (2009).
- [14] S. Augustin and C. Müller, *J. Phys. Conf. Ser.* **497**, 012020 (2014).
- [15] A. Di Piazza, E. Lötstedt, A. I. Milstein, and C. H. Keitel, *Phys. Rev. A* **81**, 062122 (2010).
- [16] A. Di Piazza, C. Müller, K. Z. Hatsagortsyan, and C. H. Keitel, *Rev. Mod. Phys.* **84**, 1177 (2012).
- [17] T. Nousch, D. Seipt, B. Kämpfer, and A. I. Titov, *Phys. Lett. B* (2016).
- [18] A. Otto, T. Nousch, D. Seipt, B. Kämpfer, D. Blaschke, A. D. Panferov, S. A. Smolyansky, and A. I. Titov, *J. Plasma Phys.* (2016).
- [19] A. Otto, D. Seipt, D. Blaschke, B. Kämpfer, and S. A. Smolyansky, *Phys. Lett. B* **740**, 335 (2015).
- [20] A. Otto, D. Seipt, D. B. Blaschke, S. A. Smolyansky, and B. Kämpfer, *Phys. Rev. D* **91**, 105018 (2015).
- [21] A. D. Panferov, S. A. Smolyansky, A. Otto, B. Kämpfer, D. B. Blaschke, and L. Juchnowski, *Eur. Phys. J. D* **70**, 1 (2016).
- [22] D. Seipt, A. Surzhykov, S. Fritzsche, and B. Kämpfer, *New J. Phys.* (2016).
- [23] T. Nousch, D. Seipt, B. Kämpfer, and A. I. Titov, *Phys. Lett. B* **715**, 246 (2012).
- [24] A. I. Titov, H. Takabe, B. Kämpfer, and A. Hosaka, *Phys. Rev. Lett.* **108**, 240406 (2012).
- [25] A. I. Titov, B. Kämpfer, H. Takabe, and A. Hosaka, *Phys. Rev. A* **87**, 042106 (2013).
- [26] A. Ringwald, *Phys. Lett. B* **510**, 107 (2001).
- [27] S. M. Schmidt, D. B. Blaschke, G. Röpke, S. A. Smolyansky, A. V. Prozorkevich, and V. D. Toneev, *Int. J. Mod. Phys. E* **7**, 709 (1998).
- [28] R. Dabrowski and G. V. Dunne, *Phys. Rev. D* **90**, 025021 (2014).
- [29] ELI, “European Extreme Light Infrastructure,” (2015), www.eli-laser.eu.
- [30] ELI-NP, “ELI Nuclear Physics,” (2015), www.eli-np.ro.
- [31] HiPER, “High Power laser for Energy Research project,” (2015), www.hiper-laser.org.

- [32] A. Ilderton, G. Torgrimsson, and J. Wårdh, Phys. Rev. D **92**, 065001 (2015).
- [33] HIBEF, “Helmholtz International Beamline for Extreme Fields,” (2015), www.hzdr.de/hgfbeamline.